VI International Conference on Computational Bioengineering
ICCB 2015
M. Cerrolaza and S. Oller (Eds)

BLOOD FLOW SIMULATIONS IN PATIENT-SPECIFIC AORTO-CORONARY BYPASS MODELS: THE ROLE OF BOUNDARY CONDITIONS

ALENA JONÁŠOVÁ*, JAN VIMMR* AND ONDŘEJ BUBLÍK*

* NTIS – New Technologies for the Information Society
Faculty of Applied Sciences, University of West Bohemia
Univerzitní 8, CZ-306 14 Pilsen, Czech Republic
e-mail: jonasova@ntis.zcu.cz, www.ntis.zcu.cz

Key words: Aorto-Coronary Bypass, Pulsatile Blood Flow, Windkessel Model, Lumped Parameter Model, Non-Newtonian Flow, Finite Volume Method

Abstract. Computer simulations of bypass hemodynamics can provide a valuable insight into the problem of graft failures, considering the close relationship between the hemodynamics and the patency and overall performance of implanted bypass grafts. However, to be able to reliably predict flow changes brought about by implanted bypass grafts, numerical simulations have to be carried out for physiologically-correct boundary conditions. In this regard, the paper demonstrates how various outlet boundary conditions (constant outlet pressure, Windkessel model and lumped parameter coronary model) can affect the quality of computed blood flow and wall shear stress distributions in relevant parts of two patient-specific aorto-coronary bypass models.

1 INTRODUCTION

In the last two decades, the computer-aided imaging methods have opened up new possibilities in diagnosis and treatment of cardiovascular disease (CVD), including the possibility to non-invasively assess the patency and overall performance of implanted bypass grafts. Besides clinical research, computational patient-specific modelling of hemodynamics is nowadays seen as a tool that has the potential to provide a valuable insight into the problem of graft failures, which are usually associated with restenosis and occlusive intimal thickening[1] (Fig. 1). In this case, the research of bypass hemodynamics is based on the (largely confirmed) hypothesis that most pathological changes are the result of post-surgical wound-healing and vessel remodelling triggered by disturbed blood flow and low and oscillating wall shear stress[1, 2].

Although computer simulations have a great potential to improve the quality of health care provided to CVD patients, their ability to give physiologically meaningful results is strongly dependent on the prescribed boundary conditions and their values. In this

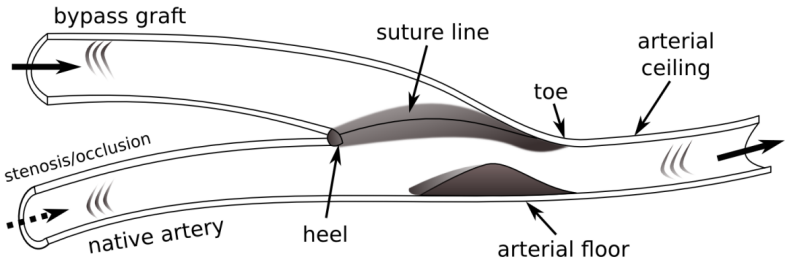

Figure 1: Sites prone to intimal thickening at a distal anastomosis[2]

context, it should be noted that according to the most recent review paper[3] on bypass hemodynamics, a considerable amount of numerical studies carried out in the past relied on the prescription of constant outlet pressures, which can, however, considerably impair the quality of obtained results. For example, in one of our latest works[4], we encountered a non-physiological phenomenon of back flow, which after detailed analysis was found out to be brought about by a reversed pressure drop originating in the prescription constant outlet pressure.

In our effort to avoid non-realistic blood flow simulations, the application of lumped parameter (0D) models[5] seems to be most promising. Thus, to confirm this assumption and to assess the extent of how coronary outlet boundary conditions can affect the results quality, the objective of the present paper is to analyse the impact of different types of outlet boundary conditions on the overall hemodynamics in patient-specific aorto-coronary bypass models (Fig. 2).

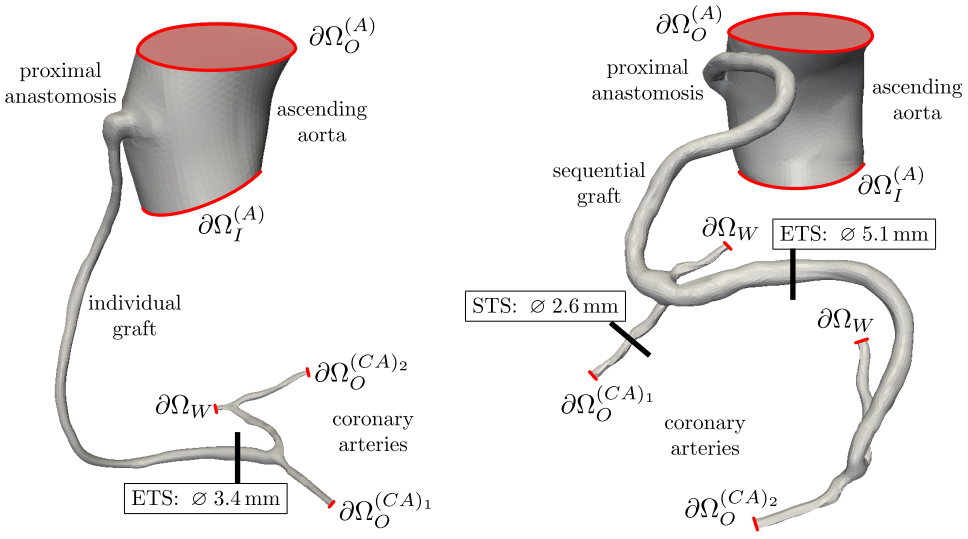

a) single bypass b) double bypass

Figure 2: Patient-specific models of single and double aorto-coronary bypasses

2 MODELS AND METHODS

Because the present hemodynamic study follows one of our earlier works[4], the modelling assumptions and simplifications adopted in this paper are based on the problem formulation described in this work. In other words, the blood flow in the aforementioned bypasses (Fig. 2) is modelled as a pulsatile laminar flow of shear-dependent fluid in static and inelastic bypass models that were reconstructed from CT scans provided by the courtesy of the University Hospital in Pilsen. The non-Newtonian behaviour of the blood is described by the Carreau-Yasuda model with corresponding parameters. For the numerical simulation of 3D pulsatile non-Newtonian blood flow, we apply our own developed and verified Navier-Stokes solver[4], algorithm of which is based on a stabilised projection method and the cell-centred finite volume method formulated for hybrid unstructured tetrahedral grids.

In accordance with the paper's objective, which is to determine the effect of three different outlet boundary conditions (see the variants a)–c) below), the same flow conditions are applied in all considered bypass models (Fig. 2):

- *aortic inlet* $\partial\Omega_I^{(A)}$ – constant time-dependent velocity profile computed on the basis of the flow rate $Q_I^{(A)}$ waveform[6] shown in Fig. 3 (left);
- *aortic outlet* $\partial\Omega_O^{(A)}$ – time-dependent outlet pressure $p_O^{(A)}$ corresponding to the pressure waveform shown in Fig. 3 (right);
- *coronary artery outlets* $\partial\Omega_O^{(CA)}$ – three different approaches are chosen:
  a) prescription of constant outlet pressure $p_O^{(CA)}$ corresponding to the average arterial blood pressure of 12 000 Pa;
  b) coupling each outlet with one three-element Windkessel model, Fig. 4 (left);
  c) coupling each outlet with one lumped parameter coronary model, Fig. 4 (right);
- *impermeable and inelastic walls, occluded proximal coronary arteries* $\partial\Omega_W$ – prescription of the non-slip boundary condition.

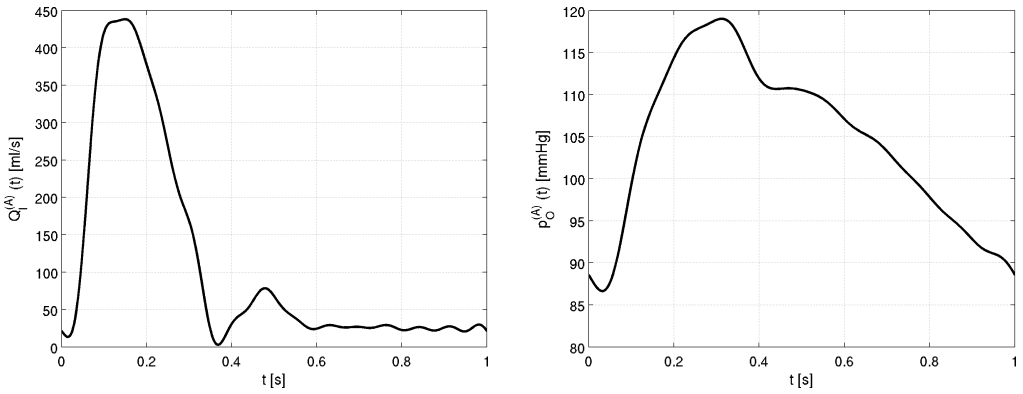

Figure 3: Flow rate (*left*) and pressure (*right*) waveforms[6] prescribed at the inlet $\partial\Omega_I^{(A)}$ and outlet $\partial\Omega_O^{(A)}$ of the ascending aorta, respectively (see Fig. 2); the cardiac cycle period is $T = 1\,\mathrm{s}$

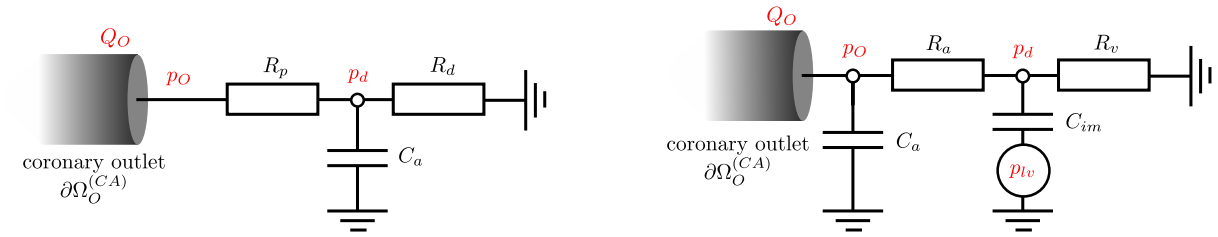

Figure 4: Schematic drawings of the three-element Windkessel model (*left*) and the coronary model (*right*) coupled to 3D bypass models via their coronary outlets $\partial\Omega_O^{(CA)}$

2.1 Windkessel model

On the basis of the electric analogue, the three-element Windkessel model (Fig. 4 (left)) applied to the outlet $\partial\Omega_O^{(CA)_s}$, $s = 1, ..., N_{out}$, where N_{out} is the number of all coronary outlets (single bypass: $N_{out} = 2$, double bypass: $N_{out} = 2$, see Fig. 2), can be represented through the following equations for the unknown pressures p_d^s and p_O^s:

$$\frac{\mathrm{d}}{\mathrm{d}t}p_d^s + \frac{1}{C_a^s R_d^s}p_d^s = \frac{1}{C_a^s}Q_O^s\,, \qquad p_O^s = p_d^s + R_p^s\,Q_O^s\,, \tag{1}$$

where p_d^s is the distal pressure (i.e., pressure in arterioles and capillaries), Q_O^s is the flow rate provided by the 3D model at the outlet $\partial\Omega_O^{(CA)_s}$, C_a^s is the capacitance and R_p^s and R_d^s are the proximal and distal resistances, respectively. The unknown pressure p_O^s, necessary for the 3D blood flow simulation, is obtained by solving Eq. (1) by means of an explicit Euler method. The parameters R_p^s, R_d^s and C_a^s used in this paper are listed in Tab. 1.

Table 1: Windkessel parameters (A is the outlet cross-sectional area)

	coronary outlets	$A \times 10^{-6}$ [m^2]	$R_p \times 10^6$ [Pa s m^{-3}]	$R_d \times 10^6$ [Pa s m^{-3}]	$C_a \times 10^{-10}$ [m^3 Pa^{-1}]
single bypass	$\partial\Omega_O^{(CA)_1}$	2.34	2 346.7	23 638.0	0.76
	$\partial\Omega_O^{(CA)_2}$	1.56	3 525.6	35 513.0	0.51
double bypass	$\partial\Omega_O^{(CA)_1}$	1.75	3 145.1	31 648.0	0.57
	$\partial\Omega_O^{(CA)_2}$	3.23	1 704.0	17 146.8	1.05

2.2 Coronary model

The simple lumped parameter model of coronary bed (Fig. 4 (right)) used in this paper is loosely based on the model introduced in the work by Sankaran et al.[7]. The most apparent difference compared to the standard Windkessel model is the fact that it incorporates the effect of the left ventricular pressure p_{lv}, which in the human body is one of the factors that give the coronary blood flow its unique waveform (the main myocardial perfusion occurs during the diastolic phase of the cardiac cycle as a consequence of

coronary artery compression during systole). Using the electric analogue, the lumped parameter model shown in Fig. 4 (right) is given by the following set of ordinary differential equations for the unknown pressures p_O^s and p_d^s:

$$\frac{\mathrm{d}}{\mathrm{d}t}p_O^s + \frac{1}{C_a^s R_a^s}p_O^s = \frac{1}{C_a^s}Q_O^s + \frac{1}{C_a^s R_a^s}p_d^s\,, \tag{2}$$

$$\frac{\mathrm{d}}{\mathrm{d}t}p_d^s + \frac{1}{C_{im}^s}\left(\frac{1}{R_a^s}+\frac{1}{R_v^s}\right)p_d^s = \frac{1}{C_{im}^s R_a^s}p_O^s + \frac{\mathrm{d}}{\mathrm{d}t}p_{lv}\,, \tag{3}$$

where R_a^s and R_v^s are the arterial and venous resistances and C_a^s and C_{im}^s arterial and intramyocardial capacitances for the coronary outlet $\partial\Omega_O^{(CA)_s}$, $s = 1, ..., N_{out}$. The values of these parameters used in the single and double bypass models are listed in Tab. 2. The numerical solution of Eqs. (2) – (3) is carried out with an explicit Euler scheme. Finally, note that besides the coronary model described in this paper, the literature offers further 0D models and modifications[8, 9].

Table 2: Parameters of the coronary model (A is the outlet cross-sectional area)

	coronary outlets	$A \times 10^{-6}$ [m^2]	$R_a \times 10^6$ [Pa s m^{-3}]	$R_v \times 10^6$ [Pa s m^{-3}]	$C_a \times 10^{-13}$ [m^3 Pa^{-1}]	$C_{im} \times 10^{-12}$ [m^3 Pa^{-1}]
single bypass	$\partial\Omega_O^{(CA)_1}$	2.34	36 847.8	11 644.7	5.93	5.02
	$\partial\Omega_O^{(CA)_2}$	1.56	55 346.1	17 490.6	3.95	3.34
double bypass	$\partial\Omega_O^{(CA)_1}$	1.75	49 237.8	15 560.2	4.44	3.76
	$\partial\Omega_O^{(CA)_2}$	3.23	26 729.0	8 447.0	8.18	6.92

As already mentioned, a crucial part of the coronary model is the inclusion of the left ventricular pressure p_{lv}. For its determination, we introduce a lumped parameter circuit model (Fig. 5) that is able to reproduce the hemodynamics of the left atrium and ventricle and supply the necessary values of p_{lv}. The contractility of the left ventricle is modelled using varying capacitance $C_{lv}(t)$ that is based on the time-varying elastance model[10]

$$E_{lv}(t) = \frac{1}{C_{lv}(t)} = \frac{p_{lv}(t)}{V_{lv}(t) - V_0}\,, \tag{4}$$

where $V_{lv}(t)$ is the volume of the left ventricle and V_0 is its 'dead' volume (i.e., volume at zero pressure). Following the work of Simaan[11], the time-varying elastance of the left ventricle is given as

$$E_{lv}(t) = (E_{max} - E_{min})\,E_n(t) + E_{min}\,, \tag{5}$$

where the constants E_{min} and E_{max} represent the minimal (diastolic) and maximal (systolic) elastances of the left ventricle, respectively, and $E_n(t)$ is the normalised time-varying

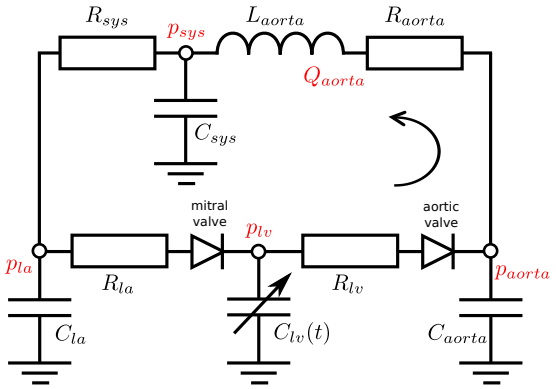

Parameters of the 0D circuit model:

$$
\begin{aligned}
R_{la} &= 333\,250\,\mathrm{Pa\,s\,m^{-3}} \\
R_{lv} &= 106\,640\,\mathrm{Pa\,s\,m^{-3}} \\
R_{aorta} &= 4\,244.3 \times 10^{3}\,\mathrm{Pa\,s\,m^{-3}} \\
R_{sys} &= 106\,640 \times 10^{3}\,\mathrm{Pa\,s\,m^{-3}} \\
C_{la} &= 3.96 \times 10^{-8}\,\mathrm{m^{3}\,Pa^{-1}} \\
C_{aorta} &= 1.08 \times 10^{-9}\,\mathrm{m^{3}\,Pa^{-1}} \\
C_{sys} &= 1.50 \times 10^{-8}\,\mathrm{m^{3}\,Pa^{-1}} \\
L_{aorta} &= 66\,650\,\mathrm{Pa\,s^{2}\,m^{-3}}
\end{aligned}
$$

Figure 5: Lumped parameter circuit model[11] with parameters tuned to the waveforms in Fig. 3 (p_{lv} – left ventricular pressure, p_{la} – left atrial pressure, p_{sys} – systemic pressure, p_{aorta} and Q_{aorta} – pressure and flow rate at the root of the ascending aorta)

elastance defined as

$$
E_n(t) = \alpha_1 \left[\frac{\left(\frac{t}{\alpha_2\, t_{max}} \right)^{\beta_1}}{1 + \left(\frac{t}{\alpha_2\, t_{max}} \right)^{\beta_1}} \right] \left[\frac{1}{1 + \left(\frac{t}{\alpha_3\, t_{max}} \right)^{\beta_2}} \right] , \tag{6}
$$

where t_{max} is the time of maximum myocardial contraction and α_i, $i = 1, 2, 3$ and β_j, $j = 1, 2$ are the model parameters. Similarly to the other two 0D models, the mathematical representation of the lumped parameter circuit model (Fig. 5) can be derived using the electric analogue, leading to the following system of ordinary differential equations

$$
\frac{\mathrm{d}\boldsymbol{x}}{\mathrm{d}t} = \boldsymbol{A}\boldsymbol{x} + \boldsymbol{B}\boldsymbol{f} , \tag{7}
$$

where $\boldsymbol{x} = [p_{lv}, p_{la}, p_{sys}, p_{aorta}, Q_{aorta}]^T$ is the vector of unknowns and

$$
\boldsymbol{A} = \begin{bmatrix}
-\frac{\dot{C}_{lv}(t)}{C_{lv}(t)} & 0 & 0 & 0 & 0 \\
0 & -\frac{1}{R_{sys}C_{la}} & \frac{1}{R_{sys}C_{la}} & 0 & 0 \\
0 & \frac{1}{R_{sys}C_{sys}} & -\frac{1}{R_{sys}C_{sys}} & 0 & \frac{1}{C_{sys}} \\
0 & 0 & 0 & 0 & -\frac{1}{C_{aorta}} \\
0 & 0 & -\frac{1}{L_{aorta}} & \frac{1}{L_{aorta}} & -\frac{R_{aorta}}{L_{aorta}}
\end{bmatrix} , \quad
\boldsymbol{B} = \begin{bmatrix}
\frac{1}{C_{lv}(t)} & -\frac{1}{C_{lv}(t)} \\
-\frac{1}{C_{la}} & 0 \\
0 & 0 \\
0 & \frac{1}{C_{aorta}} \\
0 & 0
\end{bmatrix} ,
$$

$$
\boldsymbol{f} = \begin{bmatrix}
\frac{1}{R_{la}} f(p_{la} - p_{lv}) \\
\frac{1}{R_{lv}} f(p_{lv} - p_{aorta})
\end{bmatrix} , \quad \text{where } f(y) = \begin{cases} y & \text{for } y > 0\,, \\ 0 & \text{for } y \leq 0\,. \end{cases}
$$

In this paper, the numerical solution of Eq. (6) is carried out using the four-stage Runge-Kutta method of second order accuracy in time.

To ensure that the boundary values prescribed for the coupled 3D-0D bypass-coronary model will be able to approximate the ones used with the other two types of outlet boundary conditions, the lumped parameter circuit model was tuned to reflect the flow rate and pressure waveforms shown in Fig. 3. The result of this trial-and-error tuning process is shown in Fig. 6 and was achieved with the following parameters of the time-varying elastance model: $E_{min} = 13.330 \times 10^6\,\mathrm{Pa\,m^{-3}}$, $E_{max} = 599.850 \times 10^6\,\mathrm{Pa\,m^{-3}}$, $t_{max} = 0.33 + 0.15T$, $\alpha_1 = 1.86$, $\alpha_2 = 1.4$, $\alpha_3 = 1.17$, $\beta_1 = 1.9$, $\beta_2 = 21.9$, and the circuit model parameters listed in Fig. 5. Note that the tuning process took into consideration the fact that the 3D model of the ascending aorta in both aorto-coronary bypasses is not directly adjacent to the aortic valve (the section with the coronary branches is omitted from the models), and as such the flow rate Q_{aorta} and pressure p_{aorta} generated by the lumped parameter circuit model were primarily tuned to capture the rapid ejection of blood into the aorta in the vicinity of the aortic valve (compare Q_{aorta} and $Q_I^{(A)}$ in Fig. 6).

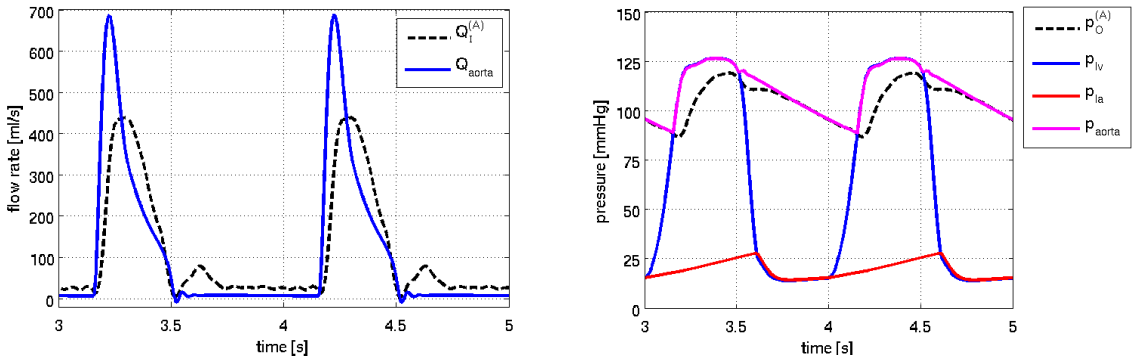

Figure 6: Flow rate (*left*) and pressure (*right*) waveforms computed by the tuned circuit model (waveforms denoted as $Q_I^{(A)}$ and $p_O^{(A)}$ are the ones shown in Fig. 3)

3 NUMERICAL RESULTS

In this paper, the results computed for the three considered outlet boundary conditions are presented with regard to blood flow waveforms and the distribution of hemodynamical wall parameters (cycle-averaged shear stress (WSS) and oscillatory shear index (OSI))[4] at relevant parts of the single and double aorto-coronary bypass models.

Besides the apparent differences in the amount of blood going through the distal anastomoses, Fig. 7 (left), the comparison of flow rate waveforms reveals the presence of back flow prior to the systolic upstroke in the case of the constant pressure. As already mentioned at the beginning of this paper, the appearance of this phenomenon, which is caused by the reversed pressure drop (see the pressure waveforms in Fig. 7 (right)), is our primary motivation for the application of 0D models in our study. That this approach is not so constraining as the one with the constant outlet pressure is confirmed by the pressure waveforms, which closely 'follow' the pressure evolution in the aorta. On the other hand, the Windkessel model fails to capture the unique flow waveforms of coronary arteries, in

a) single bypass

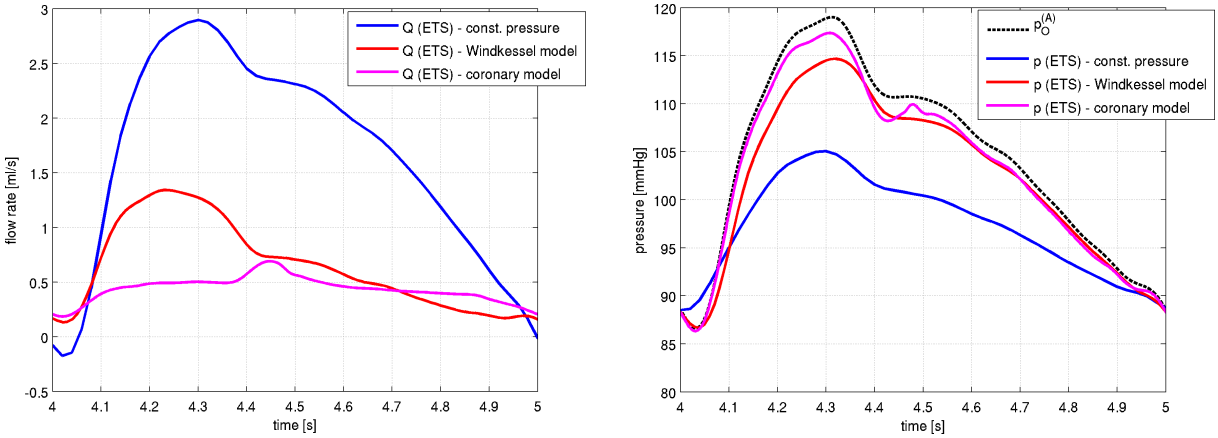

b) double bypass

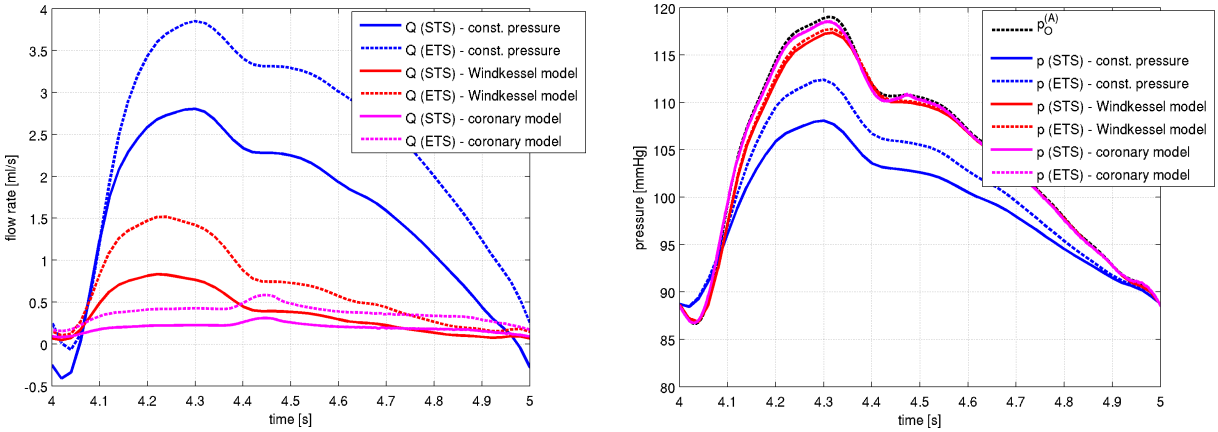

Figure 7: Flow rate and pressure waveforms at locations denoted in Fig. 2 (ETS – outflow via an end-to-side anastomosis, STS – outflow via a side-to-side anastomosis)

which the peak flow occurs during diastole. The coronary model described in Section 2.2 tries to rectify this deficiency by incorporating the effect of the left ventricular pressure as apparent from Fig. 8, where the peak flow is moved to the beginning of the diastole.

The extent of how the prescribed outlet boundary condition can affect the WSS and OSI distributions can be noted from Figs. 9 and 10, which capture the stimulation of the vessel/graft walls by the blood flow at proximal and distal anastomoses of the single and double bypass models, respectively. The considerable differences observed in both models can be clearly attributed to the previously noted decrease in blood flow associated with the application of the Windkessel as well as the coronary model (see Fig. 7). Although the introduction of the 0D models leads to a considerable decrease in WSS stimulation at both proximal and distal anastomoses (Fig. 9 (top) and Fig. 10 (left)), the elimination of back flow in the cases with incorporated 0D models contributed to a partial suppression

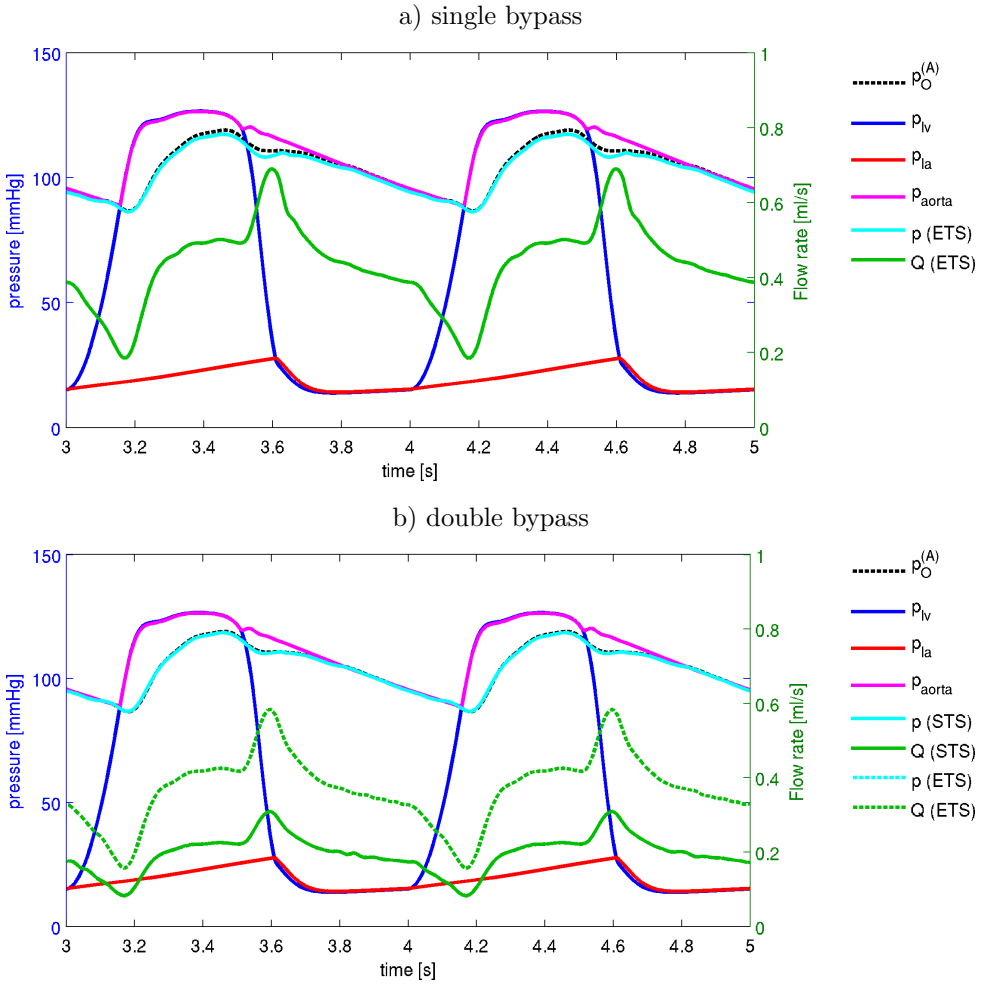

Figure 8: Pressure and flow rate waveforms computed by means of the coronary model related to the pressure waveforms of the lumped parameter circuit model

of WSS oscillations (e.g., see the OSI maps in Fig. 9 (bottom)). An exception to this can be seen in the OSI increase noted at the STS anastomosis of the double bypass, Fig. 10, which is probably caused by the complex flow field in this part of the bypass geometry.

4 CONCLUSIONS

The paper demonstrated how various outlet boundary conditions (in this case, the constant outlet pressure, the three-element Windkessel model and the lumped parameter coronary model) can affect the quality of computed flow fields and wall shear stress distributions in relevant parts of two patient-specific aorto-coronary bypass models. On the basis of the numerical results presented above, it is possible to conclude that the application of lumped parameter models as an outlet boundary condition can help to eliminate the constrains imposed by the prescription of constant outlet pressures and prevent the

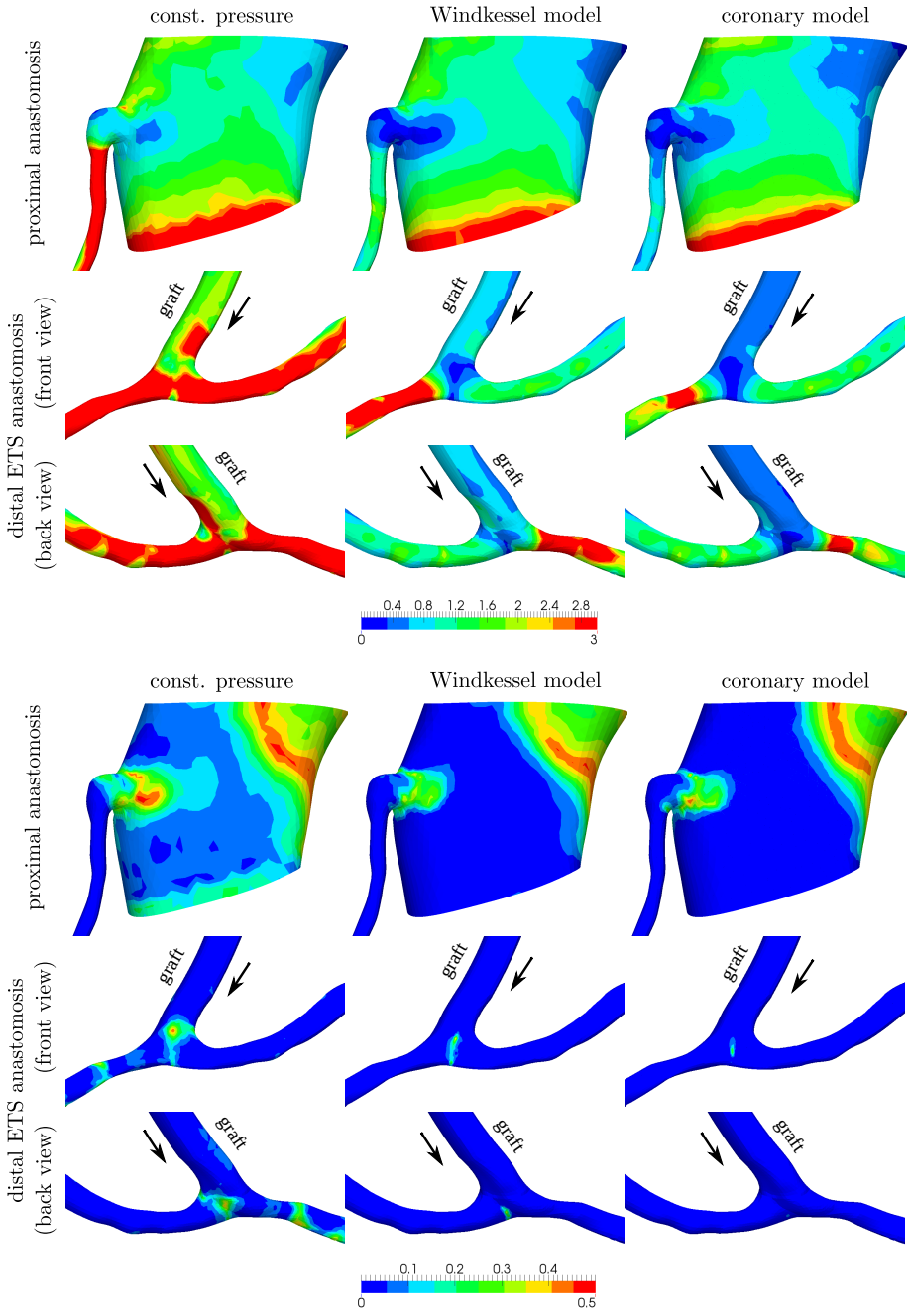

Figure 9: Effect of outlet boundary conditions on the distribution of cycle-averaged WSS [Pa] (*top*) and OSI [–] (*bottom*) in relevant parts of the single aorto-coronary bypass model

occurrence of non-realistic flow waveforms and phases of reversed pressure drop. On the other hand, the requirement of physiologically realistic waveforms placed on the coronary flow makes it necessary to introduce a special lumped parameter model that is capable to

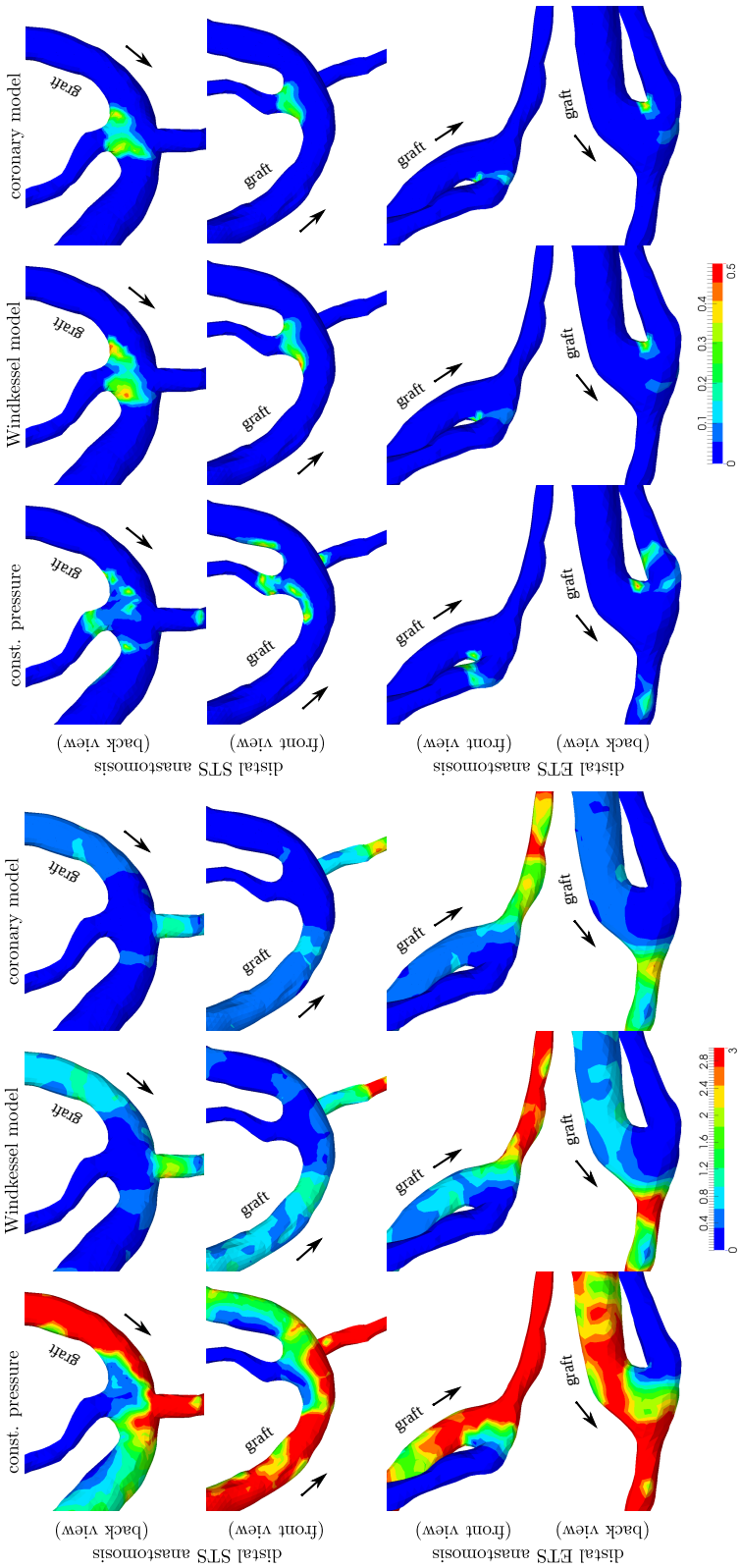

Figure 10: Effect of outlet boundary conditions on the distribution of cycle-averaged WSS [Pa] (*left*) and OSI [–] (*right*) at the side-to-side (STS) and end-to-side (ETS) anastomoses of the double aorto-coronary bypass model

incorporate the effect of the left ventricular pressure. In this paper, the coronary model coupled to a simple lumped parameter circuit model was able to provide the unique shape of real coronary waveforms in accordance with the contraction of the left ventricle, although some parameter adjustment is still necessary (especially during the later diastolic phase of the cardiac cycle).

ACKNOWLEDGEMENT

This study was supported by ERDF, project "NTIS – New Technologies for the Information Society", European Centre of Excellence, CZ.1.05/1.1.00/02.0090.

REFERENCES

[1] Haruguchi, H. and Teraoka, S. Intimal hyperplasia and hemodynamic factors in arterial bypass and arteriovenous grafts: A review. *J. Artif. Organs* (2003) **6**:227-235.

[2] Bassiouny, H.S., White, S., Glagov, S., Choi, E., Giddens, D.P. and Zarins, C.K. Anastomotic intimal hyperplasia: Mechanical injury or flow induced. *J. Vasc. Surg.* (1992) **15**:708-717.

[3] Owida, A.A., Do, H. and Morsi, Y.S. Numerical analysis of coronary artery bypass grafts: An over view. *Comput. Methods Programs Biomed.* (2012) **108**:689-705.

[4] Vimmr, J., Jonášová, A. and Bublík, A. Numerical analysis of non-Newtonian blood flow and wall shear stress in realistic single, double and triple aorto-coronary bypasses. *Int. J. Numer. Meth. Bio.* (2013) **29**:1057-1081.

[5] Kokalari, I., Karaja, T. and Guerrisi, M. Review on lumped parameter method for modeling the blood flow in systemic arteries. *J. Biomed. Sci. Eng.* (2013) **6**:92-99.

[6] Olufsen, M.S., Peskin, C.S., Kim, W.Y., Pedersen, E.M., Nadim, A. and Larsen, J. Numerical simulation and experimental validation of blood flow in arteries with structured-tree outflow conditions. *Ann. Biomed. Eng.* (2000) **28**:1281-1299.

[7] Sankaran, S., Esmaily-Moghadam, M., Kahn, A.M., Tseng, E.E., Guccione, J.M. and Marsden, A.L. Patient-specific multiscale modeling of blood flow for coronary artery bypass graft surgery. *Ann. Biomed. Eng.* (2012) **40**:2228-2242.

[8] Coogan, J.S., Humphrey, J.D. and Figueroa, C.A. Computational simulations of hemodynamic changes within thoracic, coronary, and cerebral arteries following early wall remodeling in response to distal aortic coarctation. *Biomech. Model. Mechanobiol.* (2013) **12**:79-93.

[9] Senguptam D., Kahn, A.M., Burns, J.C., Sankaran, S., Shadden, S.C. and Marsden, A.L. Image-based modeling of hemodynamics in coronary artery aneurysms caused by Kawasaki disease. *Biomech. Model. Mechanobiol.* (2012) **11**:915-932.

[10] Suga, H. and Sagawa, K. Instantaneous pressure-volume relationships and their ratio in the excised, supported canine left ventricle. *Circ. Res.* (1974) **35**:117-126.

[11] Simaan, M.A. Rotary heart assist devices. In: *Springer Handbook of Automation*, Springer Berlin Heidelberg, (2009), pp. 1409-1422.